Electrical Power and Energy Systems 57 (2014) 350–357

Contents lists available at ScienceDirect

Electrical Power and Energy Systems

journal homepage: www.elsevier.com/locate/ijepes

Analysis and assessment of VSC excitation system for power system stability enhancement

Jiawei Yang [a], Zhu Chen [a], Chengxiong Mao [a], Dan Wang [a,*], Jiming Lu [a], Jianbo Sun [b], Miao Li [b], Dahu Li [b], Xiaoping Li [b]

[a] State Key Laboratory of Advanced Electromagnetic Engineering and Technology, Huazhong University of Science and Technology, Wuhan, China
[b] Hubei Electric Power Company, Wuhan, China

ARTICLE INFO

Article history:
Received 5 September 2012
Received in revised form 4 December 2013
Accepted 10 December 2013

Keywords:
Excitation system
Power system stability
Power system damping
Transient stability

ABSTRACT

The voltage source converter (VSC) excitation system is a novel excitation system based on pulse-width modulation (PWM) voltage source converter, which is proposed as improved alternatives to the conventional thyristor excitation systems. This paper aims to provide theoretical confirmation of power system stability enhancement by the VSC excitation system. The reactive current injected to generator terminals by the VSC excitation system can be controlled flexibly. Its capability of enhancing power system stability is investigated in this paper. The simplified model of VSC excitation system suitable for use in system stability studies is developed. An extended Philips–Heffron model of a single-machine infinite bus (SMIB) system with VSC excitation system is established and applied to analyze the damping torque contribution of the injected reactive current to the power system. This paper also gives a brief explanation on why the VSC excitation system can enhance the transient stability in light of equal area criterion. The results of calculations and simulations show that the injected reactive current of VSC excitation system contributes to system damping significantly and has a great effect on the transient stability. When compared with conventional thyristor excitation systems, the VSC excitation system can not only improve the small-signal performance of the power system, but also can improve the system transient stability limit.

1. Introduction

The generator excitation system, which provides direct current to the synchronous machine field winding, is the most important and effective means to maintain the stability of power systems. Since the 1960s, the static excitation systems based thyristor converters (thyristor excitation systems) have been extensively used, for its ability of producing almost instantaneous response and high ceiling voltages. This system has a very small inherent time constant and is easily maintainable [1]. However, the modern power systems are interconnected each other to give and take the electric power and have become much more complicated than decades ago. The presence of system instability is becoming more prominent and thyristor excitation systems with conventional PSS are not sufficient to suppress the wide range (0.1–3.0 Hz) power oscillations any more. On the other hand, the long distance power transfer with heavy load seems to be more susceptive to poor damping [2]. Studies show that the thyristor excitation system cannot provide enough damping even if PSS is equipped. Furthermore, the thyristor excitation systems have following disadvantages:

(1) Commutation failure is a very frequent malfunction in thyristor converters, which is mainly caused by the ac side faults resulting in severe voltage drops [3].
(2) Thyristor converters always absorb reactive power uncontrollably in the amount of about 60% of the real power, whether the output conduction is positive or negative.
(3) The system input voltage is dependent on the terminal voltage of the generator. During system-fault conditions causing depressed generator terminal voltage, the available excitation system ceiling voltage is reduced [1]. And with only excitation control, the system stability may not be maintained if a large fault occurs close to the generator terminal [4].

Over the past decades, most of the work on excitation system focuses on exploring new control algorithms of excitation controllers, such as nonlinear control and artificial intelligence [4–8]. Little has changed about the excitation power part. With the recent development of power electronics, a novel excitation system based on pulse-width modulation (PWM) voltage source converters (VSC

* Corresponding author. Tel./fax: +86 027 8754 2669.
E-mail addresses: youngjawie@hust.edu.cn (J. Yang), wangdan@mail.hust.edu.cn (D. Wang).

0142-0615/$ - see front matter © 2013 Elsevier Ltd. All rights reserved.
http://dx.doi.org/10.1016/j.ijepes.2013.12.011

Nomenclature

δ	power angle of the generator
ω, ω_0	rotor speed and base speed
P_m	prime mover output power
P_e	active electrical power delivered by the generator
D, H	damping constant and inertia constant of the generator
E'_q, E_q	(transient) EMF in the quadrature axis
T'_{d0}	d-axis transient short circuit time constant
E_{fd}, U_{fd}	equivalent no-load EMF in the excitation coil and field voltage
V_t	generator terminal voltage
V_b	Infinite bus voltage
I_t, i_{td}, i_{tq}	stator current
x_d, x'_d	d-axis reactances
x_q, x''_q	q-axis reactances
x_T, x_L	reactance of the transformer and transmission line
L, C_{dc}	interface inductor and dc-side capacitor of the rectifier
V_{dc}	dc-side bus voltage
i_{Sabc}, i_{Sdq}	input currents of the rectifier
I_{fd}	field current
I_S	injected active current
m_d, m_q	control variables of the rectifier
d	duty ratio of the chopper
K_R	ratio of the excitation transformer
K_C	gain of the excitation amplifier

excitation system for short) has been proposed to improve the power system stability performance. The PWM converters have lots of attractive features when compared with tranditional thyristor converters, such as low harmonic distortion, bidirectional power flow, nearly sinusoidal input current, and controllable power factor [9]. Fig. 1 illustrates a typical topology of VSC excitation system, which consists of a front-end rectifier, a back-end chopper and an excitation transformer. The primary function of the rectifier is to maintain the dc capacitance voltage constant. Thus, the field voltage is regulated by the chopper only. In addition, the reactive power exchanged between the rectifier and the generator terminal can be controlled flexibly. That is to say, the VSC excitation system can not only provide field voltage like tranditional thyristor excitation systems, but also has a supplementary reactive power injector (RPI) connected in shunt with the generator terminals. The operation of the RPI is inherently fast, and with appropriate control, it can have a great effect on the alternator performance within fractions of a cycle of the normal rotor oscillation. So VSC excitation system has capacity to better maintain power system stability than tranditional thyristor excitation systems. It is worth mentioning that the performance of VSC excitation system is superior to the combination of thyristor excitation system and SVC/STATCOM. For example, the front-end rectifier is a boost converter, so the field voltage is still adequate even if the terminal voltage drops sharply. At this point, the performance of VSC excitation system is equivalent to separately excited systems. Although the VSC excitation system is expensive than tranditional thyristor excitation systems at present, it will be widely used in the near future as the cost of power electronic devices go down.

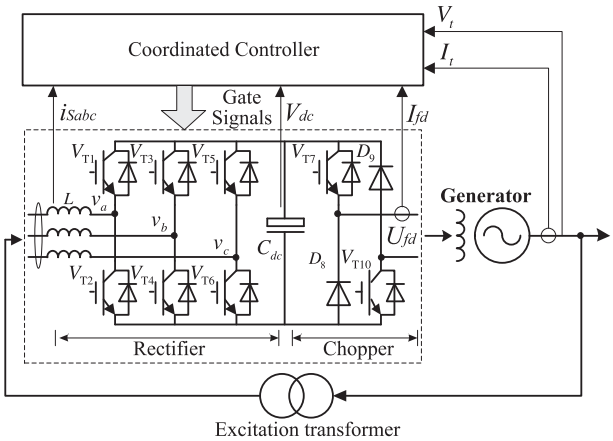

Fig. 1. Schematic of VSC excitation system.

Considerable efforts have been done to improve power system stability through regulating the field voltage in literatures [5–11]; therefore this paper concentrates on investigating the capability of the RPI to enhance power system stability. Most of the previous works on power system stability enhancement by VSC excitation system are based solely on the time-domain simulation [12–14]. This paper attempts to provide theoretic verification for the previous studies. By use of extended Philips–Heffron model, the damping torque contribution of the RPI to the power system is analyzed, so as to present an analytical explanation on why the VSC excitation system can improve system damping and small-signal stability. This paper also gives a brief investigation of the RPI effect on transient stability in light of the equal area criterion. The rest of this paper is organized as follows: Section 2 describes the simplified model of the VSC excitation system and the overall model of a single machine infinite-bus (SMIB) system installed with the VSC excitation system. The extended Philips–Heffron model and damping torque contribution of the RPI are presented in Section 3. The nonlinear simulation results of the small-signal stability improvement by VSC excitation system are also shown. In Section 4, the capability of the RPI to transient stability enhancement is evaluated. Finally, some conclusions are presented in Section 5.

2. Power system model

2.1. Simplified model of VSC excitation system

The dynamic model of the three phase rectifier corresponds to a non-linear and coupled system. Various control strategies have been proposed to get the performance of VSC improved. Fig. 2 shows the control strategy of the rectifier and chopper. The current state feedback control method [9] is employed to control the active

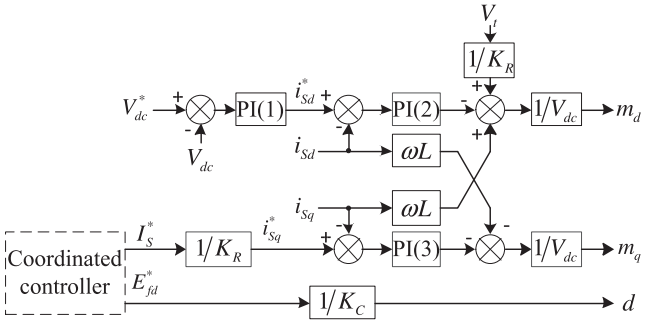

Fig. 2. The control strategy of rectifier and chopper.

and reactive current independently. For simplicity, the final relation between the controlled variables and the reference values under this strategy are linear and decoupled, as shown in (1) and (2) [15]

$$\dot{i}_{Sd} = \frac{1}{T} i^*_{Sd} - \frac{1}{T} i_{Sd} \tag{1}$$

$$\dot{i}_{Sq} = \frac{1}{T} i^*_{Sq} - \frac{1}{T} i_{Sq} \tag{2}$$

The time constant T is equal to three times PWM switching period by selecting proper parameters of rectifier current controller. It is shown that a first order dynamic response is achieved for both active and reactive currents. The active reference value i^*_{Sd} is derived from the dc-link loop (usually a PI controller), and increases with the excitation power. The active reference value i^*_{Sq} determines the reactive power injected to the generator terminals. The excitation power is only 0.25%~0.5% of generator's total power [16], so the dynamics of i_{Sd} can also be omitted. Based on that, the dynamic model of the VSC excitation system can be written as

$$\dot{I}_S = \frac{1}{T} I^*_S - \frac{1}{T} I_S \tag{3}$$

where

$$I_S = i_{Sq}/K_R \tag{4}$$

As shown by Fig. 1, when the power switches V_{T7} and V_{T10} turn on, the field voltage U_{fd} is equal to the DC voltage V_{dc}. So the synchronous generator gets positive field current. When V_{T7} and V_{T10} turn off, the direction of the field current cannot change suddenly. The diodes D_8 and D_9 allow the freewheeling current to flow. Therefore the field voltage U_{fd} is equal to $-V_{dc}$. If the duty cycle of the PWM signal for V_{T7} and V_{T10} and is d, the mean value of the field voltage could be expressed as

$$U_{fd} = (2d - 1)V_{dc} \tag{5}$$

2.2. System model

The power system studied in this paper is a single machine infinite-bus (SMIB) system, as shown by Fig. 3, which typically represents a generation station connected radially to a much larger power system. The VSC excitation system is represented by the simplified model developed above.

The dynamical equations of a synchronous generator can be expressed as follows [17]

Mechanical equations:

$$\dot{\delta} = \omega_0 \Delta\omega \tag{6}$$

$$\Delta\dot{\omega} = \frac{1}{2H}(P_m - P_e) - \frac{D}{2H}\Delta\omega \tag{7}$$

Generator electrical dynamics:

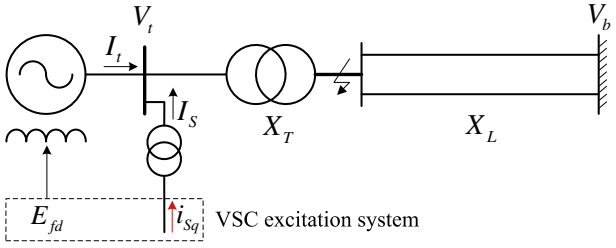

Fig. 3. The studied power system with VSC excitation system installed.

$$\dot{E}'_q = (E_{fd} - E_q)/T'_{d0} \tag{8}$$

Electrical equations:

$$P_e = E'_q i_{tq} + (x_q - x'_d) i_{td} i_{tq} \tag{9}$$

$$E_q = E'_q + (x_q - x'_d) i_{td} \tag{10}$$

$$V_t = \sqrt{(E'_q - x'_d i_{td})^2 + (x_q i_{tq})^2} \tag{11}$$

Although the third-order generator model is a simplification of the real generator, it retains the main characteristics of the power system dynamics and is widely used in designing the excitation controllers. Take account of the influence caused by the injected reactive current I_S, we can obtain that

$$\overrightarrow{V_t} = \overrightarrow{V_b} + jx_S(\overrightarrow{I_t} + \overrightarrow{I_S}) \tag{12}$$

where $x_S = x_T + x_L$.

3. Small-signal stability improvement

3.1. Extended Philips–Heffron Model

The Phillips–Heffron model of a power system has been successfully used for the analysis and design of PSS and FACTS [18–21] Although there has been considerable interest in designing excitation controller and analyzing power system stability with nonlinear models in recent years, the Phillips–Heffron model is still one of the most commonly used tools for its clear physical and engineering significance. In this section we will establish the Phillips–Heffron model of the studied power system for analysis of the damping improvement by the VSC excitation system.

Linearizing state (8)–(12) and assuming that the governor action is slow enough not to have any significant impact on the machine dynamics, we can obtain [17]

$$\Delta\dot{\delta} = \omega_0 \Delta\omega \tag{13}$$

$$\Delta\dot{\omega} = (-\Delta P_e - D\Delta\omega)/M \tag{14}$$

$$\Delta\dot{E}'_q = (\Delta E_{fd} - \Delta E_q)/T'_{d0} \tag{15}$$

$$\Delta\dot{I}_S = -\frac{1}{T}\Delta I_S + \frac{1}{T}\Delta I^*_S \tag{16}$$

where

$$\Delta P_e = K_1\Delta\delta + K_2\Delta E'_q + K_{10}\Delta I_S \tag{17}$$

$$\Delta E'_q = \frac{K_3}{1 + T'_{d0}K_3 s}(\Delta E_{fd} - K_4\Delta\delta + K_{11}\Delta I_S) \tag{18}$$

$$\Delta V_t = K_5\Delta\delta + K_6\Delta E'_q + K_{12}\Delta I_S \tag{19}$$

By substituting (17)-(19) into (13)-(15) and neglecting the inherent time constant of the RPI and field voltage, the full-state linearized model of the studied power system can be obtained as:

$$\begin{bmatrix} \Delta\dot{\delta} \\ \Delta\dot{\omega} \\ \Delta\dot{E}'_q \end{bmatrix} = \begin{bmatrix} 0 & \omega_0 & 0 \\ -\frac{K_1}{M} & -\frac{D}{M} & -\frac{K_2}{M} \\ -\frac{K_4}{T'_{d0}} & 0 & -\frac{1}{T'_{d0}K_3} \end{bmatrix} \begin{bmatrix} \Delta\delta \\ \Delta\omega \\ \Delta E'_q \end{bmatrix} + \begin{bmatrix} 0 & 0 \\ 0 & -\frac{\omega_0 K_{10}}{M} \\ \frac{1}{T'_{d0}} & \frac{K_{11}}{T'_{d0}} \end{bmatrix} \begin{bmatrix} \Delta E_{fd} \\ \Delta I_S \end{bmatrix} \tag{20}$$

It is obvious that the presence of the RPI results in a new control variable I_S while conventional thyristor excitation systems have

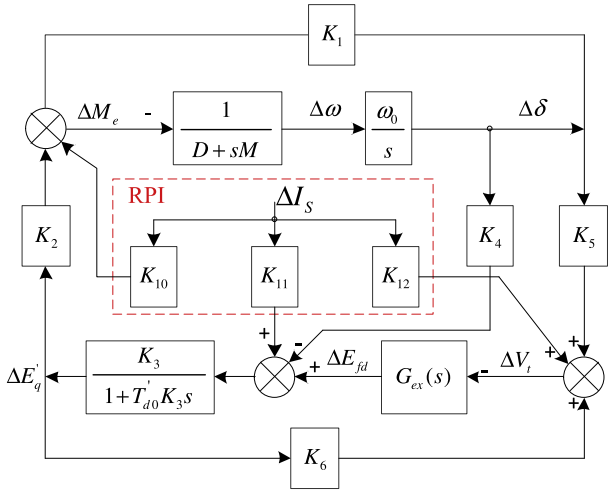

Fig. 4. The extended Philips–Heffron model of the power system.

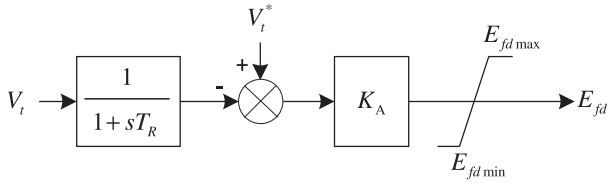

Fig. 5. Static excitation system with AVR.

only one control variable E_{fd}. From Eq. (20) we can have the extended Phillips–Heffron model of the power system installed with the VSC excitation system as shown by Fig. 4. From the block diagram, it can be found that the RPI has a component directly affecting the electromechanical oscillation loop, which is denoted by K_{10}. In addition, the RPI also contains two components indirectly affecting the electric torque, which influence the deviations in flux voltage $\Delta E'_q$ (denoted by K_{11}) and terminal voltage ΔV_t (denoted by K_{12}) respectively. In this paper, the capability of the RPI to improve power system stability will be investigated, beginning with this section on small-signal stability.

3.2. Damping torque contribution by the RPI

Damping torque analysis was first introduced for the SMIB systems by Demello and Concordia [22], and later extended to multimachine power systems for the analysis and design of the PSS or FACTS-based stabilizer in improving system oscillation stability [23–25]. For the purpose of illustration and examination of the influence on small-signal stability, the exciter model shown in Fig. 5 is considered in this paper [26]. It is representative of static excitation systems with necessary elements for a specific system. This simplifies the analysis without loss of accuracy.

Assume that the control of the RPI is of the simplest form of pure gain control. That is

$$\Delta I_S = K_\delta \Delta\delta + K_\omega \omega_0 \Delta\omega \tag{21}$$

From the block diagram of Fig. 4, the electric torque contributed by the RPI can be expressed as

$$T_e|_{\Delta I_S} = K_{10}\Delta I_S + \frac{K_2K_3(K_{11}-K_{12}K_A)}{T'_{d0}K_3s + K_3K_6K_A + 1}\Delta I_S \tag{22}$$

Usually, we have that $K_3K_6K_A \gg 1$. Then Eq. (22) can be simplified as

$$T_e|_{\Delta I_S} = K_{10}\Delta I_S + \frac{K_2(K_{11}-K_{12}K_A)}{T'_{d0}s + K_6K_A}\Delta I_S \tag{23}$$

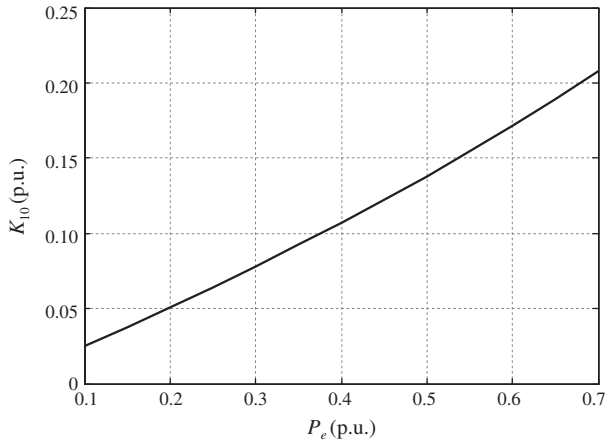

Fig. 6. Variation of K_{10} with P_e.

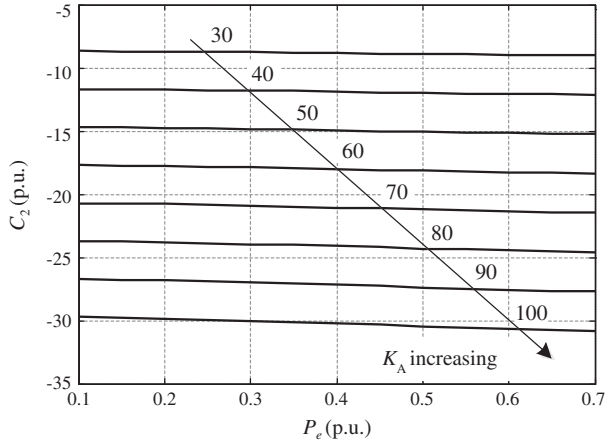

Fig. 7. Variation of C_2 with P_e for various values of K_A.

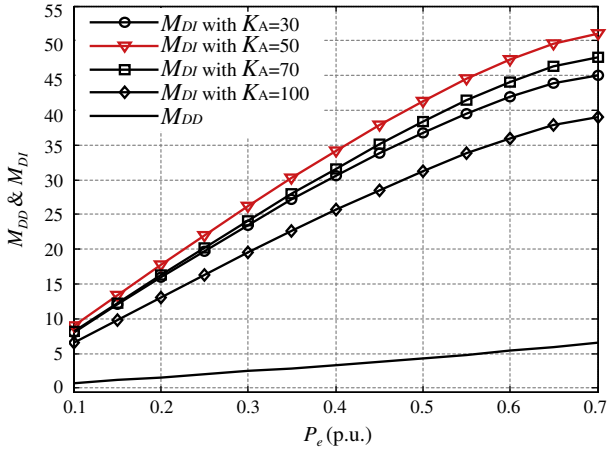

Fig. 8. M_{DD} and M_{DI} contribution by the RPI.

Hence, the damping torque coefficient due to the RPI is

$$M_D|_{\Delta I_S} = \underbrace{K_{10}K_\omega\omega_0}_{M_{DD}}\Delta\omega + \underbrace{C_1C_2(K_\omega K_6K_A - K_\delta T'_{d0})\omega_0}_{M_{DI}}\Delta\omega \tag{24}$$

where

$$C_1 = \frac{K_2(K_{11}-K_{12}K_A)}{(K_6K_A)^2 + (\omega T'_{d0})^2} \tag{25}$$

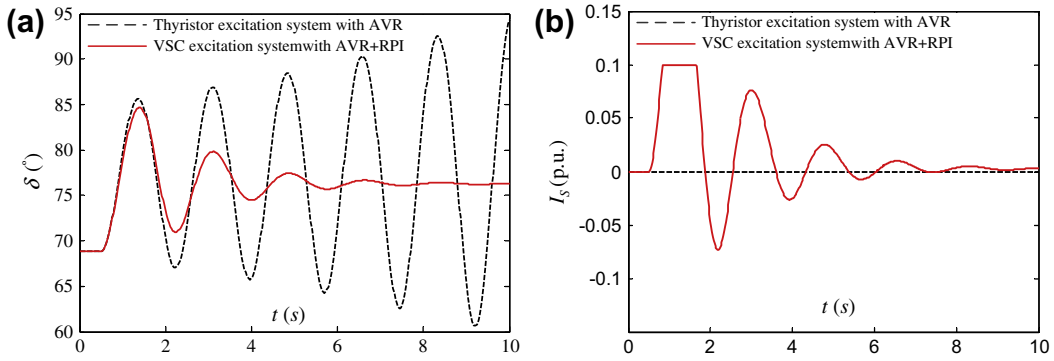

Fig. 9. System responses for a 5% step change in P_m.

$$C_2 = K_{11} - K_{12}K_A \tag{26}$$

The first component of Eq. (24) is termed as the "direct damping torque" [22], which directly applies to the electromechanical oscillation loop of the generator and is mainly measured by coefficient K_{10}. The second component is termed as the "indirect damping torque", which applies through the field channel of the generator and is related to the deviation of field voltage caused by the RPI. The parameters K_2, K_3, K_4, K_6 and C_1 are usually positive [1]. Therefore whether the RPI deteriorates or aids the system damping is primarily influenced by K_{10}, K_{11}, K_{12} and the exciter gain K_A.

Variations of parameters K_{10} and C_2 are plotted by varying generator power P_e from 0.1 p.u. to 0.7 p.u. (the power limit of the transmission lines is 0.76 p.u.) for various values of K_A by keeping the terminal voltage V_t and infinite bus voltage V_b at 1.0 p.u. The SMIB system is a weak system with long distance transmission lines [16] and the parameters are given in Appendix C. Figs. 6 and 7 show the variation of K_{10} and C_2 respectively, with P_e. For all foreseeable operating conditions, K_{10} is always positive while C_2 is always negative. Thus, the effect of the RPI on damping torque component is determined by the RPI control parameter K_δ and K_ω. Eq. (24) indicates that if $K_\omega > 0$ and $K_\omega K_6 K_A < K_\delta T'_{d0}\omega_0$, the direct damping torque coefficient M_{DD} and the indirect damping torque coefficient M_{DI} are both positive. That is, the RPI provides the power system with a positive damping.

Fig. 8 shows the variation the direct and indirect damping torque coefficient contributed from the RPI with the control parameters $K_\delta = 9.0$, $K_\omega = 0.1$ at typical machine oscillating frequencies of about 1.0 Hz. Observe that for given control parameters, the direct damping torque coefficient M_{DD} and the indirect damping torque coefficient M_{DI} are both positive over the whole range of operating and system conditions and they increase with the increasement of P_e. And it can be observed that the indirect damping torque coefficient M_{DI} is much greater than the direct damping torque coefficient M_{DD}. This is because the effect of ΔI_S is amplified as much as K_A times by the exciter before it forms the indirect damping torque, as can be seen from Fig. 4.

In order to demonstrate these results more accurately, the nonlinear simulations of the example SMIB system in terms of the rotor angle δ for a 0.05 p.u. step change in prime mover output power P_m are shown by Fig. 9. The system is operated with (a) thyristor excitation system with AVR ($K_A = 50.0$) and (b) VSC excitation system with AVR + RPI ($K_A = 50.0$, $K_\delta = 0.9$, $K_\omega = 0.1$). The system is unstable with AVR alone. The system becomes stable with additional RPI and the system oscillation is damped quickly. From the simulation results and the above analyses, it is readily apparent that the RPI can improve power system damping significantly.

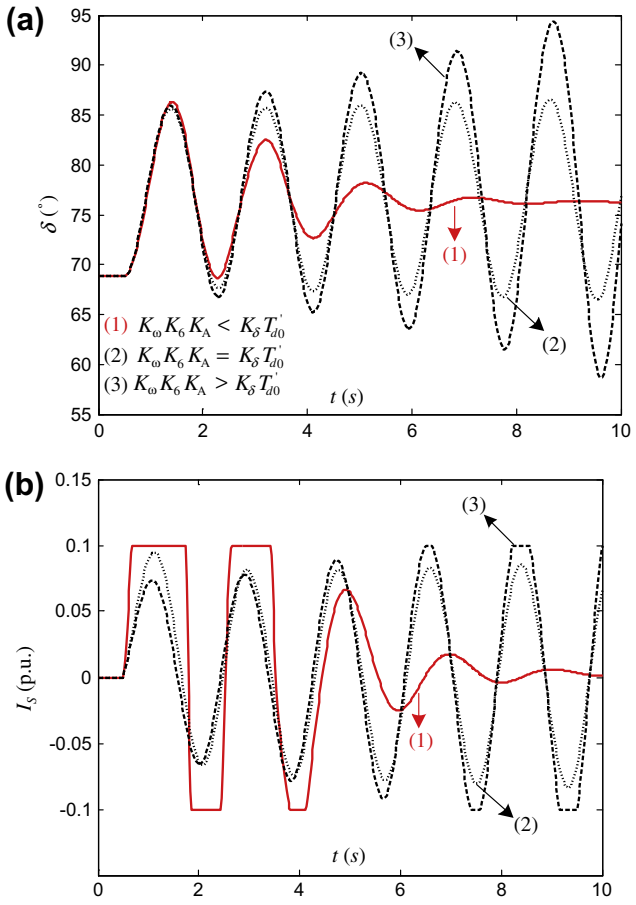

Fig. 10. System responses under different RPI control parameters.

3.3. Influence of the RPI control parameters

Equation (24) also implies a criterion on whether the RPI control provides power systems with positive or negative damping torque. Higher value of K_ω is beneficial in increasing direct damping torque coefficient M_{DD}. However, in so doing it may result in negative indirect damping torque coefficient M_{DI}. For M_{DD} is usually much smaller than M_{DI}, the condition of damping torque contribution by the RPI can be expressed as

$$\begin{cases} K_\omega K_6 K_A < K_\delta T'_{d0}, & \text{positive damping} \\ K_\omega K_6 K_A > K_\delta T'_{d0}, & \text{negative damping} \end{cases} \tag{27}$$

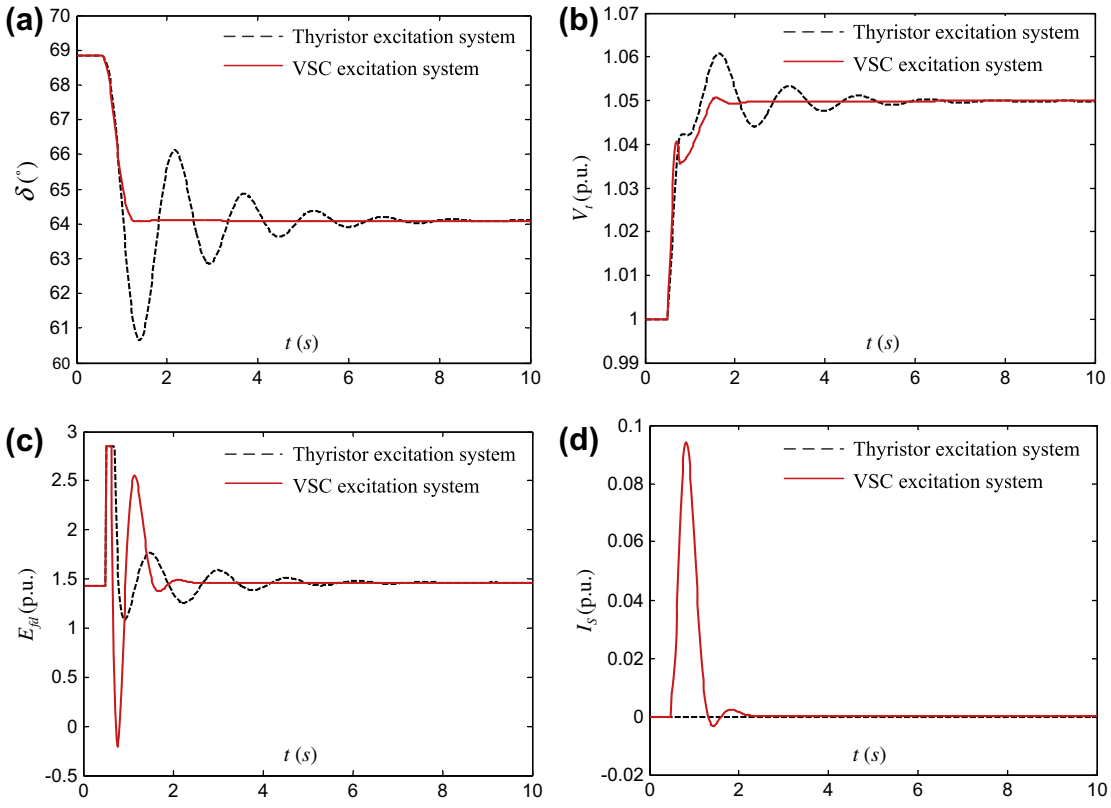

Fig. 11. System responses for a 5% step increase in the terminal reference voltage.

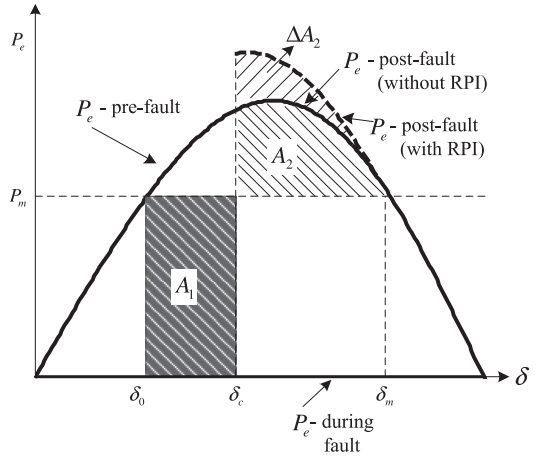

Fig. 12. The effect of the RPI on transient stability.

Fig. 10 shows the simulation results for a 0.05 p.u. step change in prime mover output power P_m under three sets of RPI control parameters:

(1) $K_\omega = 0.1, K_\delta = 6.6 \quad (K_\omega K_6 K_A < K_\delta T'_{d0})$
(2) $K_\omega = 0.1, K_\delta = 0.6 \quad (K_\omega K_6 K_A = K_\delta T'_{d0})$
(3) $K_\omega = 0.1, K_\delta = 0.1 \quad (K_\omega K_6 K_A > K_\delta T'_{d0})$

The gain K_A of the AVR is fixed at 50.0 so that the influences of the exciter are almost the same. It is observed from Fig. 10 that $K_\omega K_6 K_A = K_\delta T'_{d0}$ can be interpreted as a critical condition of the effect of the RPI on damping torque. When $K_\omega K_6 K_A < K_\delta T'_{d0}$, the system oscillation is damped, while when $K_\omega K_6 K_A > K_\delta T'_{d0}$, the oscillation becomes more intensely and the generator loses synchronism at last. These results are consistent with the analyses above and give design basis for the RPI control parameters.

3.4. Small-signal stability improvement

A small disturbance in the terminal reference voltage is considered to investigate the effectiveness of the VSC excitation system. The terminal reference voltage is increased by a step of 5% at $t = 0.5$ s. The performance of the VSC excitation system is compared with the results of a thyristor excitation system controlled by conventional AVR + PSS. The parameters of the PSS which are shown to give the best performance in [16] are given as follows:

$$T_q = 4s, K_S = 1.0, T_1 = T_3 = 2s, T_2 = 0.638s, T_4 = 0.824s$$

A coordinated controller based on linear optimal control (LOC) theory is developed in this paper. Although many nonlinear controllers for coordinating excitation and FACTS devices are proposed in literatures, they have strict requirements of system parameters. LOC is a simple and effective method to design coordinated controllers, and has been widely used for generator excitation in China. The design procedure is shown in Appendix B. The control law of VSC excitation system in the simulations is

$$\begin{bmatrix} \Delta E_{fd} \\ \Delta I_S \end{bmatrix} = \begin{bmatrix} 50 & -8 & 40 \\ -0.65 & -0.1 & 2.5 \end{bmatrix} \begin{bmatrix} \Delta P_e \\ \Delta\omega \\ \Delta V_t \end{bmatrix} \tag{28}$$

Fig. 11 illustrates the simulation results of conventional thyristor excitation system and proposed VSC excitation system, where the generator angle, terminal voltage, field voltage and injected active power of VSC are respectively demonstrated. With tranditional thyristor excitation system, the number of generator active power oscillation is more than three, which means the corresponding damping coefficient is less than 0.159 [17]. However, through injecting a capacitive reactive current to generator terminal, the VSC excitation system makes the power system restore stabilization quickly. It is clear the first rotor angle swing is significantly reduced and the number of power oscillation is close to one. That is to say

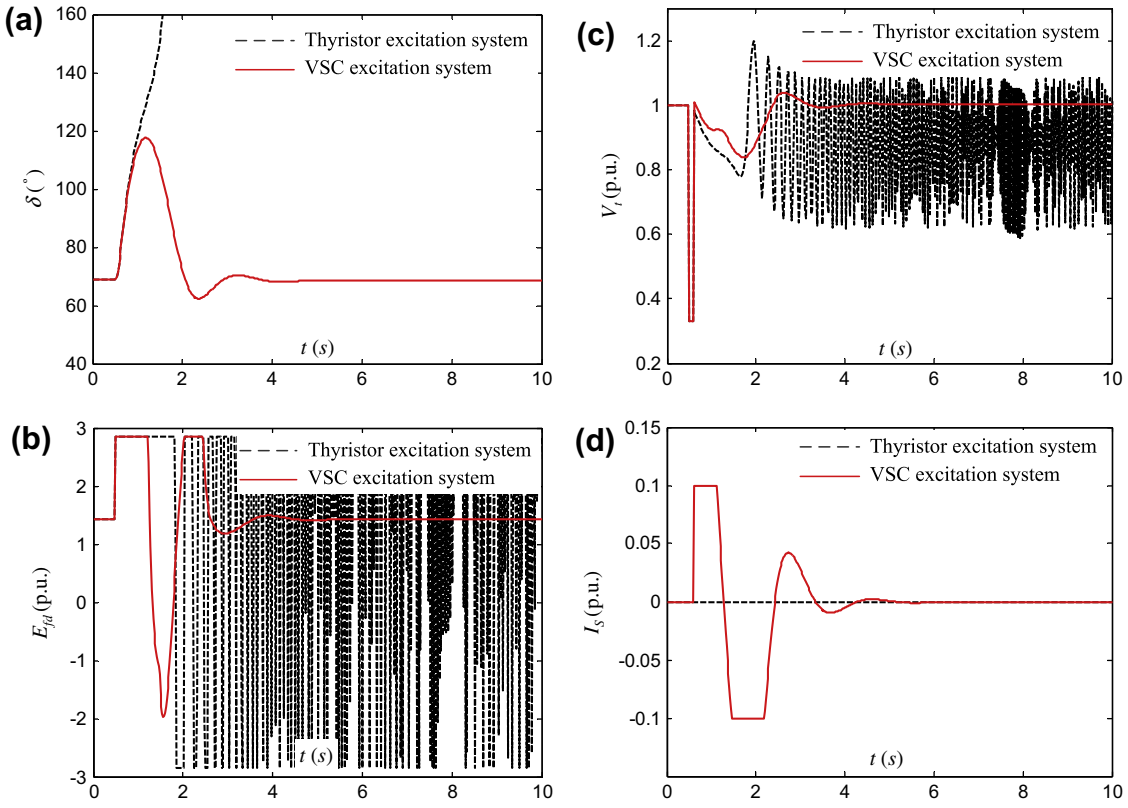

Fig. 13. System responses for a three-phase fault.

the damping coefficient is marked up to 0.477. Therefore there is no doubt that the proposed VSC excitation system is much better than the tranditional thyristor excitation system in improving power system small-signal stability.

4. Transient stability improvement

Since there is no inertia in power electronics conversion process, the injected reactive current of VSC excitation system can be changed very rapidly within the limits set. This feature can be used to dynamically modulate the system reactive power to increase the stability margins in the system.

This issue can be further clarified in light of the equal area criterion. For the system shown in Fig. 3, the P–δ relationship can be obtained from (13)-(15)

$$P_e = \frac{E'_q V_b}{x'_{d\Sigma}} \sin\delta + \frac{1}{2}\frac{(x'_d - x_q)V_b^2}{x'_{d\Sigma}x_{q\Sigma}} \sin 2\delta \tag{29}$$

where

$$x'_{d\Sigma} = x'_d + x_S - x'_d x_S I_S / V_t \tag{30}$$

$$x_{q\Sigma} = x_q + x_S - x_q x_S I_S / V_t \tag{31}$$

It is clear that the change of the injected reactive current I_S will alter the P–δ curve of a power system. When the reactive current is capacitive ($I_S > 0$), system P–δ curve is raised; when the reactive current is inductive ($I_S < 0$), system P–δ curve is lowered. Let us consider the effect of the RPI to a three-phase to ground fault at the outlet of the step-up transformer, as shown in Fig. 3. The fault in cleared after 100 ms. Fig. 12 shows P–δ plots for the three network conditions: (i) pre-fault (steady state), (ii) during fault (with a three-phase fault), and (iii) post-fault (fault is cleared). It is well-know that if the decelerating area A_2 is less than the accelerating area A_1, the kinetic energy gain during the accelerating period cannot be completely expended, and the stability will be lost.

As shown by Fig. 12, if the VSC excitation system injects a capacitive reactive current after the fault has been cleared, the system P–δ curve is raised. Thus, the decelerating area is expanded to $A_2 + \Delta A_2$. Thereby the first swing instability can be avoided. It is very meaningful when the generator is loaded heavily. Fig. 13 shows the simulation results when the system subjected to the three-phase fault that we discussed. The active power of the generator is close to the power limitation. It is obvious that the system with thyristor excitation system is first-swing unstable. The addition of the RPI contributes to maintain first-swing stability and the oscillation of the system with proposed VSC excitation system is damped quickly. It is evident from these results and above discussions that the VSC excitation system can maintain transient stability more effectively than tranditional thyristor excitation system.

5. Conclusion

The VSC excitation system is proposed as alternatives to the conventional thyristor excitation systems, which enhances oscillation damping and improves transient dynamics of power systems. It has two approaches to maintain power system stability: the field voltage and the reactive power injector (RPI). The dynamic response of RPI is extremely quickly, in milliseconds, while the response time of field voltage is usually seconds. The results of damping torque calculations and simulations show that the RPI contributes to system damping significantly, thus the small-signal performance of the power system is improved. What's more, the RPI also enhances the transient stability limit pronouncedly. Therefore the generator can transmit more active power to power systems. For power systems which have the need of improving damping and the transmission capacity, the use of VSC excitation system will be an advantageous solution.

Acknowledgment

This work was supported by the National Natural Science Foundation of China (No. 50977035).

Appendix A. The parameters of the extended Philips–Heffron model of the SMIB system with VSC excitation system

$$K_1 = \frac{(x_q - x'_d) i_{q0} V_b \sin\delta_0}{x'_{d\Sigma}} + \frac{E'_{Q0} V_b \cos\delta_0}{x_{q\Sigma}} \tag{A-1}$$

$$K_2 = i_{q0} \frac{x_{q\Sigma}}{x'_{d\Sigma}} \tag{A-2}$$

$$K_3 = \frac{x'_{d\Sigma}}{x_{d\Sigma}} \tag{A-3}$$

$$K_4 = \frac{(x_d - x'_d) V_b \sin\delta_0}{x'_{d\Sigma}} \tag{A-4}$$

$$K_5 = \frac{v_{td0} x_q V_b \cos\delta_0}{x_{q\Sigma} V_{t0}} - \frac{v_{tq0} x'_d V_b \sin\delta_0}{x'_{d\Sigma} V_{t0}} \tag{A-5}$$

$$K_6 = \frac{v_{tq0} x_S}{x'_{d\Sigma} V_{t0}} \tag{A-6}$$

$$K_{10} = \frac{x_S}{V_{t0}^2} \frac{x'_d}{x'_{d\Sigma}} \frac{E'_{q0} V_b \sin\delta_0}{x'_{d\Sigma}} - \frac{x_S}{V_{t0}^2} \frac{V_b^2}{2} \frac{(x_q - x'_d)}{x'_{d\Sigma} x_{q\Sigma}} \left(\frac{x'_d}{x'_{d\Sigma}} + \frac{x_q}{x_{q\Sigma}} \right) \sin 2\delta_0 \tag{A-7}$$

$$K_{11} = \frac{(x_d - x'_d) x_S v_{tq0}}{x'_{d\Sigma} V_{t0}^2} \tag{A-8}$$

$$K_{12} = \frac{x_S}{V_{t0}^3} \left(\frac{x_q v_{td0}^2}{x_{q\Sigma}} + \frac{x'_d v_{tq0}^2}{x'_{d\Sigma}} \right) \tag{A-9}$$

Appendix B. Linear optimal excitation controller (LOEC) design

Since E'_q and δ are difficult to be measured in practice, E'_q is replaced by V_t and δ is replaced by P_e in (20). Then we get the state equations expressed as

$$\dot{\mathbf{x}} = \mathbf{A}\mathbf{x} + \mathbf{B}\mathbf{u} \tag{B-1}$$

where

$$\begin{cases} \mathbf{x} = [\,\Delta P_e \quad \Delta\omega \quad \Delta V_t\,]^T \\ \mathbf{u} = [\,\Delta E_{fd} \quad \Delta I_S\,]^T \end{cases} \tag{B-2}$$

Based on linear optimal control theory, under the performance index

$$J = \frac{1}{2} \int_0^\infty (\Delta\mathbf{x}^T \mathbf{Q} \Delta\mathbf{x} + \Delta\mathbf{u}^T \mathbf{R} \Delta\mathbf{u}) dt \tag{B-3}$$

where $\mathbf{Q}$ and $\mathbf{R}$ are weight matrices.

The optimal control law is

$$\mathbf{u} = -\mathbf{K}\mathbf{x} \tag{B-4}$$

and

$$\mathbf{K} = \mathbf{R}^{-1}\mathbf{B}^T\mathbf{P} \tag{B-5}$$

where $\mathbf{P}$ is the solution of the Riccati equation

$$\mathbf{A}^T\mathbf{P} + \mathbf{P} - \mathbf{P}\mathbf{B}\mathbf{R}^{-1}\mathbf{B}^T\mathbf{P} + \mathbf{Q} = 0 \tag{B-6}$$

Appendix C. Parameters of the example power system

Generator:

$$x_d = 1.03,\ x_q = 0.6,\ x'_d = 0.39,\ T'_{d0} = 6s, H = 7.6s,\ D = 0.05$$

Transmission Line:

$$x_T = 0.16,\ x_L = 1.15$$

References

[1] Kundur P. Power system stability and control. New York: McGraw-Hill, Inc; 1994.
[2] Zhu F, Liu Z, Chu L. Achievement and experience of improving power system stability by pss/excitation control in china. In: IEEE power engineering society general meeting; 2004. p. 1767–71.
[3] Thio CV, Davies JB, Kent KL. Commutation failures in hvdc transmission systems. IEEE Trans Power Del 1996;11:946–57.
[4] Youyi W, Hill DJ, Middleton RH, et al. Transient stability enhancement and voltage regulation of power systems. IEEE Trans Power Syst 1993;8:620–7.
[5] Zhu C, Zhou R, Wang Y. A new nonlinear voltage controller for power systems. Int J Electr Power Energy Syst 1997;19:19–27.
[6] Chengxiong M, Malik OP, Hope GS, et al. An adaptive generator excitation controller based on linear optimal control. IEEE Trans Energy Convers 1990;5:673–8.
[7] Leon AE, Solsona JA, Valla MI. Comparison among nonlinear excitation control strategies used for damping power system oscillations. Energy Convers Manage 2012;53:55–67.
[8] Fusco G, Russo M. Nonlinear control design for excitation controller and power system stabilizer. Control Eng Pract 2011;19:243–51.
[9] Ye Y, Kazerani M, Quintana VH. A novel modeling and control method for three-phase PWM converters. In: IEEE 32nd annual power electronics specialists conference; 2001. p. 102–7.
[10] Talaq J. Optimal power system stabilizers for multi machine systems. Int J Electr Power Energy Syst 2012;43:793–803.
[11] He P, Wen F, Ledwich G, et al. Effects of various power system stabilizers on improving power system. Int J Electr Power Energy Syst 2013;46:175–83.
[12] Chengxiong M, Jiandong W, Huibi L, et al. Large synchronous generator excitation system based on current source converters. Water Resources and Power 2008;3:172–5.
[13] Lina H, Chengxiong M, Jiming L, et al. Novel excitation system using high power electronics full controlled devices rectifier. High Voltage Eng 2009;35:1711–7.
[14] Jiawei Y, Jiandong W, Chengxiong M, et al. Study on the excitation system based on full-controlled-devices for improving power system damping characteristics. Large Electr Mach Hydraul Turb 2012:63–7.
[15] Wu R, Dewan SB, Slemon GR. A PWM ac-to-dc converter with fixed switching frequency. IEEE Trans Ind Appl 1990;26:880–5.
[16] Qu L. Power system stability and generator excitation control. Beijing: China Electric Power Press; 2007.
[17] Yu YN. Electrical power system dynamics. NewYork: Academic Press Inc.; 1983.
[18] Heffron WG, Phillips RA. Effect of a modern amplidyne voltage regulator on underexcited operation of large turbine generators. IEEE Trans Power Appl Syst 1952;71:692–7.
[19] Swift FJ, Wang HF. The connection between modal analysis and electric torque analysis in studying the oscillation stability of multi-machine power systems. Int J Electr Power Energy Syst 1997;19:321–30.
[20] Liu C, Yokoyama R, Koyanagi K, et al. PSS design for damping of inter-area power oscillations by coherency-based equivalent model. Int J Electr Power Energy Syst 2004;26:535–44.
[21] Pandey RK, Singh NK. Upfc control parameter identification for effective power oscillation damping. Int J Electr Power Energy Syst 2009;31:269–76.
[22] DeMello FP, Concordia C. Concepts of synchronous machine stability as affected by excitation control. IEEE Trans Power Appl Syst 1969;PAS-88:316–29.
[23] Wang HF, Swift FJ. Application of the Phillips-Heffron model in the analysis of the damping torque contribution to power systems by svc damping control. Int J Electr Power Energy Syst 1996;18:307–13.
[24] Larsen EV, Swann DA. Applying power system stabilizers part I: general concepts. IEEE Trans Power Appl Syst 1981;PAS-100:3017–24.
[25] Marshall WK, Smolinski WJ. Dynamic stability determination by synchronizing and damping torque analysis. IEEE Trans Power Appl Syst 1973;PAS-92:1239–46.
[26] IEEE recommended practice for excitation system models for power system stability studies. 1992.